Optical characterization of highly conductive single-wall carbon-nanotube transparent electrodes

T. M. Barnes,[1] J. van de Lagemaat,[1] D. Levi,[1] G. Rumbles,[1] T. J. Coutts,[1] C. L. Weeks,[2] D. A. Britz,[2] I. Levitsky,[2]
J. Peltola,[2] and P. Glatkowski[2]

[1]*National Renewable Energy Laboratory, Golden, Colorado 80401, USA*
[2]*EIKOS Inc., Franklin, Massachusetts 02038, USA*

We report on a complete characterization of the optical dispersion properties of conducting thin films of single-wall carbon nanotubes (SWCNTs). The films studied exhibit sheet resistances between 50 and 1000 Ω/sq and optical transparencies between 65% and 95% on glass and quartz substrates. These films have the potential to replace transparent conducting oxides in applications such as photovoltaics and flat-panel displays; however, their optical properties are not sufficiently well understood. The SWCNT films are shown to be hole conductors, potentially enabling their use as hole-selective contacts and allowing alternative device designs. The fundamental optical, morphological, and electrical characteristics of the films are presented here, and a phenomenological optical model that accurately describes the optical behavior of the films is introduced. Particular attention is paid to ellipsometry measurements and thorough evaluation of the reflection and absorption spectra of the films.

PACS number(s): 78.67.Ch, 73.63.Fg, 78.20.Ci

I. INTRODUCTION

Thin films of transparent conductive materials have a wide variety of industrially important applications, including photovoltaics (PV), flat-panel displays, and touch screens.[1] These materials are generally metal oxides such as In_2O_3:Sn (ITO), ZnO:Al, or SnO_2:F, which are called transparent conducting oxides (TCOs). ITO has the best combination of optical and electrical properties of the commonly used TCOs; however, it would be beneficial to replace ITO in many applications due to its cost and brittleness. The optoelectronic properties of ZnO and SnO_2 are adequate for many applications, but their use is limited due to issues with stability and patterning.[1] Almost all TCO materials are strongly *n*-type, and a transparent *p*-type or hole-conducting contact would be desirable for thin-film PV.[2] A non oxide transparent electrical contact with the potential to be hole conducting, flexible, low cost, and simple to deposit would be highly beneficial for the next generation of PV devices.

Several groups have proposed replacing traditional TCOs with thin films made of single-wall carbon-nanotube (SWCNT) networks.[3–6] These SWCNT films can be deposited successfully on flexible substrates using low-cost, low-temperature deposition methods. One major advantage of the SWCNT films over TCOs such as ITO, ZnO, and SnO_2 is that their fabrication process readily produces a preferentially hole-conducting contact.[3] This is particularly advantageous in organic PV devices, and we have achieved efficient devices in which the SWCNT network replaces both ITO and poly(3,4-ethylenedioxythiophene) poly(styrenesulfonate) (PEDOT:PSS) in a typical bulk heterojunction device.[7] Others have also had success replacing the ITO layer in a bulk heterojunction device on a flexible substrate.[8] We have also successfully replaced the ZnO bilayer in an efficient $CuIn_2Se_3$/CdS device.[9] Previous work on *p*-GaN indicates that SWCNT network electrodes can produce an ohmic contact to a *p*-type semiconductor.[10]

Bulk SWCNTs contain a random distribution of differing lengths, diameters, and chiralities. This distribution generally consists of about two-thirds semiconducting tubes and one-third metallic tubes. The tubes can be made by a variety of methods including chemical-vapor deposition, laser ablation of a graphite target, and electric-arc decomposition of a target. As produced, the tubes are intermixed with large amounts of amorphous carbon and metallic impurities, both of which must be removed before the tubes are used for electronic applications.[11] A variety of purification procedures are in use, but most rely on an acid reflux that can unintentionally (but often beneficially) dope the *p*-type semiconducting tubes.[12] This, along with doping from atmospheric impurities,[13] is thought to influence the optoelectronic performance of the films.

Conductivities in SWCNT networks are quite different from conductivities observed in individual SWCNTs, and the conduction mechanism in networks has been a topic of discussion in several recent works.[14–16] The conductivity was found to be affected by several factors, including network density,[16,17] interactions between tubes or bundles,[16,17] bundle length,[14] and doping.[18] In Ref. 16, it was observed that conduction in SWCNT networks can be dominated by either metallic or semiconducting tubes depending on the density of the network. Transport in "thin," or lower density, networks was observed to be dominated by semiconducting tubes with the metallic tubes functioning as interconnects, with Schottky barriers at the interconnects controlling the resistivity. Transport in "thick" networks, which can be as thick as 35 μm for a 50 Ω/sq film, was controlled by interconnected metallic tubes.[16]

In comparison with Ref. 16, it is difficult to determine whether metallic or semiconducting SWCNTs dominate the resistivity in the networks studied in this work. These networks are thin in terms of their optical transparency and physical thickness, but with a sheet resistance more typical of thick networks or "buckypaper." Earlier work showed that conductivity within a SWCNT rope exhibits both metallic and semiconducting characteristics.[15] These ropes showed a semiconducting temperature dependence of resistivity at low temperatures and a metallic temperature dependence at high

temperatures. The transition temperature between the two regimes increased with the degree of tangling in the rope.[19] Network conductivity also increases with bundle length[14] and is strongly affected by doping.[12,18] This combined set of data suggests that the conduction mechanism in SWCNT networks is complex and difficult to describe in terms of a single conductivity type. We study the conductivity of the networks discussed in this work to facilitate comparison with previous work and determine if the observed electrical properties are consistent with the optical characterization results.

Although the SWCNT network electrodes described here and elsewhere have important potential advantages over traditional TCOs, their optical performance requires substantial improvement for many applications. Research on transparent conducting SWCNT films is still quite recent,[3,20] and most earlier studies of SWCNT optical properties focused on their behavior in liquid dispersions, opaque films, and freestanding buckypapers. This work enabled the identification of fundamental transitions leading to optical absorption due to Van Hove singularities in the SWCNT density of states and the π-plasmon resonance. The transition due to the Van Hove singularities is known as the E_s^{11}, E_s^{22}, and E_m^{11} transitions, and they were associated with optical absorptions close to 0.7, 1.3, and 1.8 eV.[21] A strong, broad optical loss centered around about $4-5$ eV has been associated with the π-plasmon resonance of the SWCNTs.[21–23] The π plasmon arises from a collective excitation of the π-electron system of the SWCNTs, with an especially strong contribution from the metallic tubes.[24] This phenomenon limits transparency in the visible range, which is of great importance for photovoltaics. All of these features are known to shift in wavelength depending on doping, tube bundling, measurement technique, and the tube growth and purification method.[20] In this work, we study the optical properties of commercially available, highly conductive and transparent SWCNT network electrodes in an effort to understand the optical loss mechanisms affecting their performance.

II. EXPERIMENT

The fabrication of transparent conductive films of single-walled carbon nanotubes has been described previously.[25,26] Single-walled carbon nanotubes were produced using the arc discharge method from Ni-Y packed graphite rods. The nanotubes were found to have an average diameter of 1.43 nm, based on transmission electron microscopy, Raman, and near-infrared spectroscopies. This diameter is typical of nanotubes produced using the arc discharge method. Soot from the arc reactor was purified using a combination of acid reflux, washing, and centrifugation.[27,28] This process removed the majority of metal catalyst particles and nontubular carbon. The remaining material consists of a mixture of approximately 1/3 (semi-) metallic and 2/3 semiconducting tubes. The purified SWCNTs were dispersed in water and alcohol with the aid of sonication to form a stable dispersion. The dispersion was spray coated onto heated microscope glass or quartz substrates.[25] After drying, the resulting coating consisted of essentially pure SWCNTs. The morphology of these coatings can be described as a randomly distributed
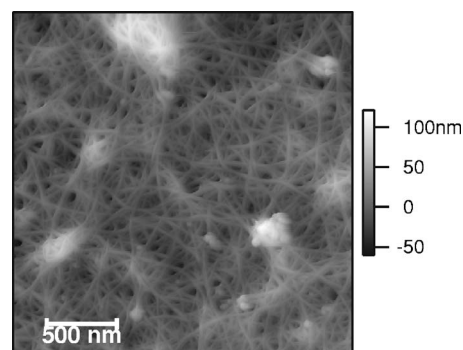

FIG. 1. AFM image of a typical 50 Ω/sq SWCNT network on quartz. This film is 40 nm thick with an rms roughness of 31 nm.

network of SWCNT bundles with a high density of void space.

In this work, we characterized a set of SWCNT films using the techniques traditionally applied to TCO characterization to evaluate their optoelectronic performance and suitability as a replacement for TCOs in a variety of applications. Film thickness was determined optically using ellipsometry in conjunction with atomic force microscopy (AFM). Morphology and composition were further evaluated using scanning electron microscopy (SEM) and energy-dispersive x-ray spectroscopy (EDS). Additional compositional analysis was performed using Auger electron spectroscopy (AES) and x-ray photoelectron spectroscopy (XPS).

The electrical resistivity of the films was evaluated using a four-point probe, and the conductivity type was determined with Seebeck effect measurements on a custom-built and reference calibrated system.[29] Hall-effect and temperature-dependent conductivity measurements were conducted on a Bio-Rad HL5500 Hall-effect system. The optical transmission and reflection were studied using a Cary 5G UV-VIS-NIR spectrophotometer between 250 and 2500 nm using an integrating sphere to account for diffusely scattered light. A Woollam M-2000 variable-angle spectroscopic ellipsometer (VASE) was used to measure the refractive index and extinction coefficient of the SWCNT networks on quartz and glass substrates. We show the spectral dependence of the optical constants, which are critical parameters for optical device engineering. In addition to performing ellipsometry measurements, the VASE was also used for angularly dependent reflection and normal-incidence transmission measurements. A large set of SWCNT networks with sheet resistances between 50 and 1000 Ω/sq was characterized in this study, with a focus on the most conductive $50-100$ Ω/sq films.

III. RESULTS AND DISCUSSION

A. Morphology and composition

Figure 1 shows an AFM image of a 50 Ω/sq SWCNT film on quartz. Thickness measurements were made on this and other films by imaging over an area with a scratch from a razor blade. Line averaging over 2 μm of a 50 Ω/sq layer yielded a thickness of 40 nm with a root-mean-square (rms) roughness of $\pm$31 nm. The 100 Ω/sq film was 30 nm thick

with an rms roughness of ±26 nm. Based on the measured sheet resistances and thickness, we calculated a coarse volume conductivity on the order of 3300 to 5000 S/cm. Due to significant void space and high rms roughness of the SWCNT network, the volume conductivity of such SWNCT films is difficult to determine quantitatively. This volume conductivity is on the order of typical TCOs (Ref. 30) and is orders of magnitude higher than that of PEDOT:PSS, a commercially available transparent conducting polymer.[31] Particles as tall as 240 nm were found on both films. Profilometry and SEM cross-section measurements produced erroneously high thickness measurements because the films are so thin and rough. SEM combined with EDS showed some of the particles to be primarily carbonaceous. No metallic impurities were detected with EDS, AES, or XPS in any of the films.

B. Electrical properties

A four-point probe was typically used to measure the sheet resistance of each film between 50 and 1000 Ω/sq. Although conductivity measurements were simple on these films, evaluating transport properties of the films was found to be nontrivial. Several Hall-effect measurements were performed on both the custom-built and BioRad HL5500 systems to determine the carrier density and mobility. Both systems yielded unreasonable values for the carrier density between 10^{21} and 10^{23} cm^{-3} with very large experimental errors. The Hall-effect measurement was also unable to reliably determine the carrier type. The effective mobility (0.04–0.3 cm^2/V-s in our measurements) in the networks appears to be too low to yield a reasonable Hall- or Nernst-effect measurement. The low mobility could be caused by several factors including high resistivity between SWCNT bundles and Schottky barriers between semiconducting and metallic nanotubes.[32] Additionally, Hall-effect measurements are intended for use on thin films and bulk materials. We caution future researchers about using Hall-effect measurements for SWCNT films, since using the data could be misleading.

Figure 2(a) shows the temperature dependence of the resistivity for a typical SWCNT network. The measurements were carried out while heating the sample from 100 to 450 K. The network resistivity shows an initial decrease as the temperature increases up to about 200 K. This decrease in resistivity as temperature increases is commonly observed in semiconductors. However, the resistivity then slowly increases up to 275 K and increases more sharply above 325 K. SWCNT networks are known to exhibit a crossover between nonmetallic and metallic conductivities at a critical temperature that varies between 210 and 250 K for mats and ropes.[33] Several factors, including dedoping,[13,34] onset of metallic conduction,[19] or a reduction of the van der Waals forces in the tube bundles with temperature that limits intertube conductivity,[16] could be contributing to the increase in resistivity with temperature above 200 K. These results suggest that conduction in these networks is neither purely metallic nor purely semiconducting.

Figure 2(b) demonstrates that the Seebeck effect measurements show a positive slope with very little error. This indi-
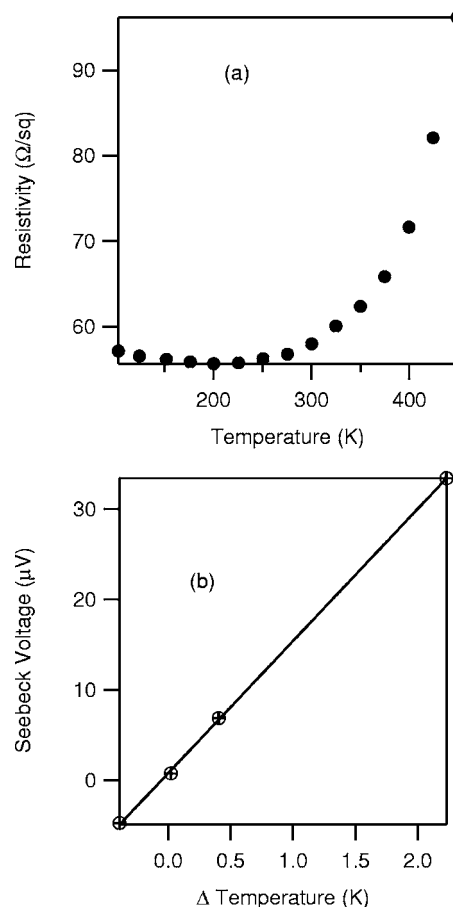

FIG. 2. (a) Resistivity as a function of temperature indicates a minimum resistivity at 225 K with a sharp increase at elevated temperatures. (b) Seebeck voltage as a function of temperature variation across a 2 cm substrate for a 50 Ω/sq film on glass. The positive Seebeck coefficient indicates a hole-conducting material.

cates that the networks are hole conducting, again indicating the potential importance of semiconducting nanotubes or indicating that the metallic tubes can act as semimetals. The measurement yields a Seebeck coefficient of 16.5±1.4 μV/K, which is in agreement with previous results for SWCNT samples.[18,35] Seebeck measurements are less sensitive to low carrier mobility than Hall measurements and, therefore, are more reliable than Hall measurements for determining carrier sign. Previous work has shown that the Seebeck coefficient of SWCNTs is influenced by ambient gases, depending on their molecular mass.[35] The results presented here were measured in vacuum, and they would be expected to change in magnitude, but not in sign, depending on the measurement ambient. Further evidence for the hole-selective conductivity of SWCNT networks is abundant in the literature. The standard oxidative purification process is known to induce p-type charge-transfer doping of the nanotubes,[3] and several groups have observed that SWCNT networks behave like p-type semiconductors in field effect transistors.[36,37] PV,[7] organic light-emitting diode (LED),[38] and inorganic LED (Ref. 10) devices have successfully used SWCNT networks as hole-selective contacts. Additionally, SWCNT networks show strong signs of rectifying contact in
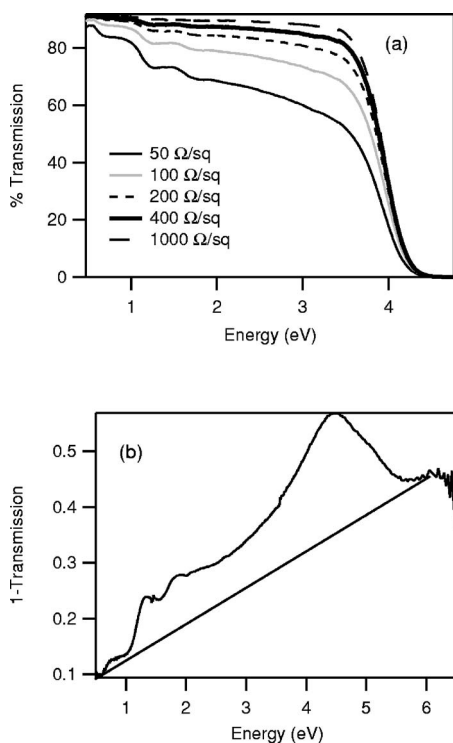
FIG. 3. (a) Optical transmission of bare SWCNT networks on glass as a function of sheet resistance varying from 50 to 1000 Ω/sq and wavelength. (b) shows the approximated absorbance calculated from $1-T$ for a 50 Ω/sq film on quartz. The line was used to perform a linear subtraction for peak fitting as described in Ref. 22.

applications where *n*-type semiconductors are normally employed.[9]

C. Optical properties

Figure 3(a) shows the optical transmission of the SWCNT networks as a function of sheet resistance. For more conductive films with sheet resistances between 50 and 100 Ω/sq, the optical transparency is between 60% and 80% in the visible range due to absorption in the SWCNT network. However, the transparency is considerably higher at energies below 1.1 eV (1100 nm), which is where the optical transparency of traditional TCOs degrades due to free-carrier absorption.[1] High transparency at long wavelengths combined with high conductivity would be beneficial in thin-film tandem solar cells.[2] The more resistive networks (200–1000 Ω/sq) exhibit extremely high transparency (>80%) throughout the visible and near IR. The SWCNT networks are also much thinner than most TCO layers; therefore, the transmission spectrum shown here lacks the strong interference fringes that are often evident in TCO transmission spectra. This leads to much more uniform transmission through the SWCNT network.

Absorption spectra can be determined simply by subtracting the transmission and reflection spectra from unity. Reflection data are often neglected in this calculation to yield an approximated absorption spectrum, but it is not known if this is an acceptable approximation for SWCNT films. Following the procedure given in the literature,[22] an approximated absorption spectrum calculated from transmission data taken on the Cary spectrophotometer is shown in Fig. 3(b). There is a small peak in this spectrum at around 0.7 eV and a distinct peak at 1.3 eV. These are close to the expected locations for the E_{11}^s and E_{22}^s transitions of the SWCNT, which vary with size distribution and synthesis method.[20,21] The E_{11}^m transition at 1.8 eV is difficult to resolve in this spectrum. The E_{11}^s, E_{22}^s, and E_{11}^m peaks are weak, indicating that the semiconducting SWCNTs are doped.[3] There is a large peak around 4.4 eV that corresponds to the π-plasmon resonance of the metallic SWCNTs. This peak can shift by more than 1 eV depending on measurement technique and whether the SWCNTs are in a film or dispersed in solution. A single Lorentzian oscillator fitted to the peak after a linear background subtraction indicates a peak position for the π plasmon of 4.46 eV. This is identical to the peak position reported for a SWCNT film sprayed from an acetone solution in Ref. 22. However, this assignment does not provide any information on whether the decrease in transmission at the π plasmon occurs because of absorption or reflection losses. The approximated absorption spectra from the SWCNT network films show strong qualitative similarities with absorption spectra from SWCNT dispersed in solutions, and the quantitative differences between them will contain information on how bundling, network formation, and doping (unintentional or intentional) affect the optoelectronic properties of the films.

Spectroscopic ellipsometry measurements were performed at 50°, 60°, and 70° angles of incidence, along with plane-polarized transmission measurements. Ellipsometry measures the change in polarization upon reflection from a surface. The polarization change is expressed in terms of two quantities, Ψ and delta Δ. Ψ is related to the ratio of the reflection amplitudes of the *s* and *p* polarizations, whereas Δ is the phase change between the two polarizations. The optical constants were fitted using the WVASE32 software package.[39] Glass and quartz substrates were used for ellipsometry, and the data presented here are from films on quartz substrates. The optical constants of the quartz substrates were fitted separately using a standard Cauchy model and incorporated into the composite model for the film and substrate. All of the data were backside corrected to account for the reflection at the back of the transparent substrate. The film thicknesses were initially fixed in the model at 40 and 30 nm, respectively, for the 50 and 100 Ω/sq films. They were then allowed to vary in the final model, leading to values of 39.8 nm for the 50 Ω/sq film and 22.78 nm for the 100 Ω/sq film, which is in reasonable agreement with the AFM data shown in Fig. 1. A Maxwell-Garnett effective medium approximation was used to model the void fraction in the films. AFM and SEM indicated a void fraction close to 30% in the SWCNT films and a very high surface roughness. To prevent parameter correlation, the void fraction at the substrate was held fixed at 30% for both conductivities and was allowed to vary linearly toward the top surface to account for surface roughness. The model found void fractions at the surface of 85% for the 50 Ω/sq film and 87% for the 100 Ω/sq film. This approach was used in place of an explicit surface roughness layer.

TABLE I. Fitting parameters for the ellipsometric data. G in the table indicates a Gaussian oscillator, and G-L indicates a Gauss-Lorentzian (or Voigt) oscillator. Amp. is the amplitude and B is the broadening. Oscillators 1–3 correspond to the semiconducting and metallic transitions of the SWCNT, and oscillator 6 represents the π-plasmon peak from the metallic SWCNTs.

Oscillator	Amp.	Energy	B	B_{mix}	B_L	B_G
G 1	2.3214	0.7669	0.3701			
G 2	1.5451	1.3361	0.3545			
G 3	0.4106	1.8190	0.3143			
G 4	0.7242	1.9019	0.9699			
G 5	1.8611	2.8154	3.3954			
G-L 6	3.3590	4.6104	0.9908	1.087	0.9389	0.3166
G 7	1.6908	6.6114	3.4512			

The optical model for the SWCNT layer was built using a generalized oscillator or "genosc" layer in the WVASE32 software. This technique models the imaginary part of the dielectric function as a sum of analytic oscillator functions and calculates the real part of the dielectric function from the imaginary part using a Kramers-Kronig transformation. The custom-developed dielectric function for the SWCNT consists of six Gaussian contributions plus a single peak described by a convolution of a Gaussian and Lorentzian (Voigt) peak. The functional form of the complex dielectric constant generated from the genosc model is given in Eq. (1). The first term in Eq. (1) is a purely real constant, and the second is a pole oscillator included to account for the effect of absorptions outside the measured spectral range on the real part of the dielectric function. The third term is the contribution of six Gaussian oscillators to the dielectric function,

$$\widetilde{\varepsilon} = \varepsilon_{1,offset} + \frac{A_{n,pole}}{E_n^2 - E^2} + \left(\sum_{n=1}^{6} \mathrm{Gaussian}(A_n, E, B_n) \right)$$
$$+ [G - L(A_n, E, B_n, B_{mix}, B_L, B_G)]. \tag{1}$$

The analytic Gaussian expression for ε_2 is given in Eq. (2a). Equation (2b) contains the Kramers-Kronig integration yielding the Gaussian contribution to ε_1 and the addition of ε_2 to produce the complete complex contribution from the Gaussian oscillator,

$$\varepsilon_{n,2} = A_n \exp\left[-\left(\frac{2\sqrt{\ln(2)}E - E_n}{\mathrm{Br}_n} \right)^2 \right]$$
$$- A_n \exp\left[-\left(\frac{2\sqrt{\ln(2)}E + E_n}{\mathrm{Br}_n} \right)^2 \right], \tag{2a}$$

$$\widetilde{\varepsilon} = \sum_{n=6} \frac{2}{\pi} \left[P \int_{R_G}^{\infty} \xi \frac{\varepsilon_{n,2}(\xi)}{\xi^2 - E^2} d\xi + i(\varepsilon_{n,2}) \right]. \tag{2b}$$

The fourth term in Eq. (1) is the Gauss-Lorentzian contribution to the dielectric function, which was developed by Kim et al.[40] Unlike the Gaussian oscillator, which is an analytic function, this is a Kramers-Kronig consistent numerical approximation.

Equation (3a) gives the functional form of the Gauss-Lorentzian contribution. Equations (3b)–(3d) describe the

parameters used in the integration. B_L and B_G in Table I correspond to Γ_n and σ_n, respectively, from Eqs. (3b)–(3d),

$$\widetilde{\varepsilon} = iA_n \left\{ \int_0^{\infty} e^{i[E-E_n+i\gamma_n(s)]s} ds - \int_0^{\infty} e^{i[E+E_n+i\gamma_n(s)]s} ds \right\}, \tag{3a}$$

$$\gamma_n(s) = \Gamma_n + 2\sigma_n^2 s, \tag{3b}$$

$$\mathrm{Br}_n^2 = \Gamma_n^2 + \sigma_n^2, \tag{3c}$$

$$e^{B_{mix,n}} = \Gamma_n / \sigma_n. \tag{3d}$$

In each equation, A_n is a unique constant in each term, E represents energy, Br is a broadening term, and B_{mix} indicates the relative Gaussian and Lorentzian contributions to the G-L oscillator. The best-fit model parameters for these equations are presented in Tables I and II.

This model was developed phenomenologically based on fits to the ellipsometry data. Standard models for transparent conductors, such as the Drude[41] model, could not fit the optical data satisfactorily. WVASE32 uses the Levenburg-Marquardt algorithm to minimize the mean squared error (MSE) between the measured and calculated Ψ and Δ values.[42] The optical model was fitted to both the ellipsometry and transmission data simultaneously. The MSE for the 50 Ω/sq films was 10.03, and the MSE for the 100 Ω/sq film was 10.58 using this model. The MSE could be reduced to 5 for the 50 Ω/sq film when fitting only to the ellipsom-

TABLE II. Linear offset and pole fitting parameters for the ellipsometric model. These parameters consist of a real constant (ε_1) and two pole oscillators to account for the effect of absorption outside the measured spectral range on the dispersion function.

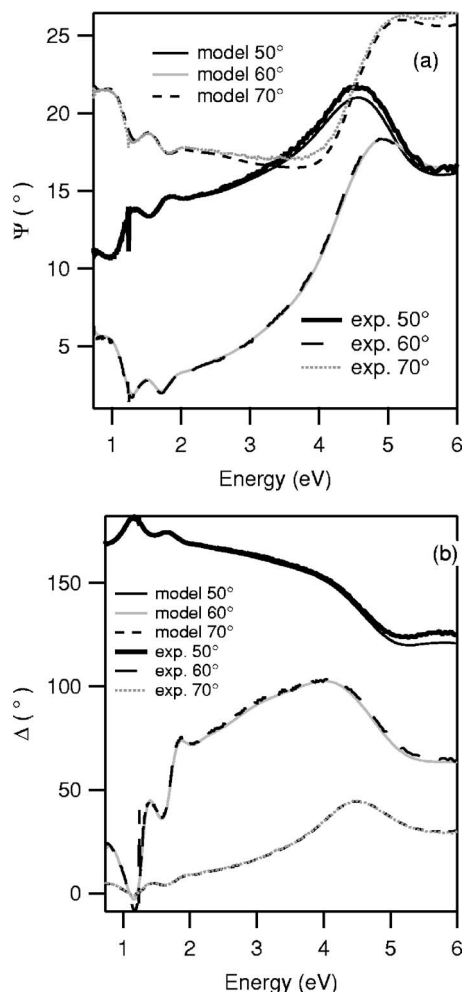| Term	Value
ε_1 offset	2.9557
Pole 1 position	11
Pole 1 magnitude	0
Pole 2 position	0.4157
Pole 2 magnitude	1.9117

FIG. 4. Experimentally measured and modeled (a) Ψ and (b) Δ as a function of energy at 50°, 60°, and 70° angles of incidence for a 50 Ω/sq SWCNT films on quartz. These fits were used to generate the optical constants, and the predicted transmission, reflection, and absorption spectra in WVASE32 that are shown in Figs. 5–7.

FIG. 5. Real (ε_1) and imaginary (ε_2) dielectric constants as a function of energy for 50 and 100 Ω/sq films. The values of the optical constants completely overlap for the 50 and 100 Ω/sq films. The optical constant values were determined from fits to spectroscopic ellipsometry and plane-polarized transmission measurements. Peak assignments are from Refs. 20 and 21.

etry data, instead of fitting both the ellipsometry and transmittance data. The fitting procedure enforced Kramers-Kronig consistency. Figure 4 illustrates the good agreement between the measured and model-predicted (a) Ψ and (b) Δ data. SWCNTs are known to exhibit optical anisotropy,[43–45] but the degree of anisotropy in bundled and networked tubes is not well understood. The model presented in this work represents an isotropic approximation for the optical properties of the SWCNT networks.

Figure 5 shows the optical constants as a function of energy for 50 and 100 Ω/sq films. The optical constants are identical for SWCNT network films up to 200 Ω/sq, which is different from previous results reporting a change in the magnitude of the optical constants with thickness and conductivity.[4] We do not expect a difference in the optical constants for these films because they are all deposited from a common ink and differ only in thickness, and not in volume fraction or density of SWCNTs. Optical constants could not be determined for the higher-sheet-resistance layers due to the low reflectivity of the extremely thin SWCNTs layers. The optical constants show a strong spectral dependence,
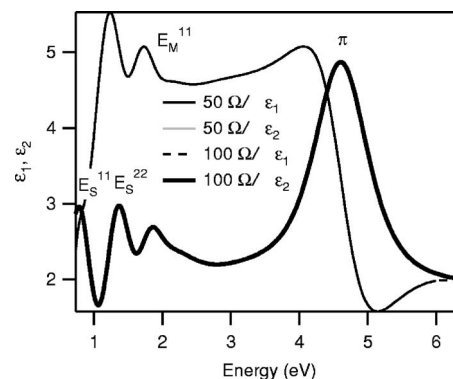
with intense peaks corresponding to the fundamental transitions of the SWCNT. The strong peak in ε_2 at 4.75 eV can be attributed to the π-plasmon resonance of the metallic nanotubes,[22] leading to very low transmission at short wavelengths. The two semiconducting transitions at 0.7 and 1.3 eV and the metallic transition at 1.8 eV could degrade the optical transparency of the electrodes significantly in the range of interest for photovoltaics. These peaks also correspond to several of the oscillators in the model that are shown in Table I. The first three Gaussian oscillators in the table correspond to the fundamental semiconducting and metallic transitions of the SWCNT, and the Gauss-Lorentzian oscillator corresponds to the π-plasmon resonance of the metallic tubes. The remaining oscillators generate the background absorption in the imaginary part of the dielectric function. As stated above, the optical model is phenomenological, and the functional forms of the oscillators are not assigned any physical significance.

There are strong correlations between the ellipsometry and transmission data for these films. The E_{11}^s and E_{22}^s peaks have nearly identical energies when measured with either technique. The location of the E_{11}^M peak is similar, but the peak is more easily seen with ellipsometry. The ellipsometry data indicate that there should be a significant reflection in the spectral region associated with the π plasmon. Figure 5 shows a large peak in ε_2 coinciding with a sharp decrease in ε_1, which corresponds to a peak in reflectance around 4.6–5 eV. Most authors determine absorption in SWCNTs materials simply from the transmission data, but this may not be appropriate for thin films of SWCNTs. The magnitude and spectral shape of both ε_1 and ε_2 agree well with the low-energy portions of the spectrum derived from electron-energy-loss spectroscopy data.[24] Additionally, ε_1 remains positive and nonzero throughout this range, which suggests that the networks do not behave as purely metallic conductors at room temperature. This is in agreement with the results from the temperature-dependent resistivity study.

Figure 6 illustrates the measured (a) reflectance, (b) transmittance, and (c) absorption from the Cary spectrophotometer, along with WVASE model predictions for the transmis-
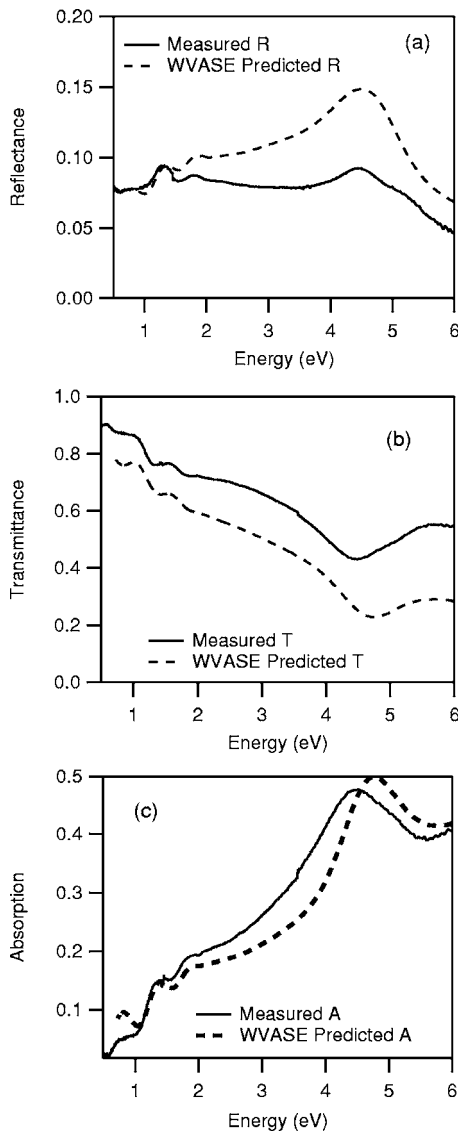
FIG. 6. (a) Reflection, (b) transmission, and (c) absorption spectra for a 50 Ω/sq SWCNT film on quartz. (a) Measured reflection spectra (solid line) with the WVASE-model-predicted reflectance (dotted line) as a function of energy. (b) Measured transmission spectra with the WVASE-model-predicted transmission spectrum. (c) Measured absorption spectrum $(A = 1 - T - R)$ with the WVASE-model-predicted spectrum. The WVASE model data were generated from the optical constants shown in Fig. 5.

sion and reflection for a 50 Ω/sq film on quartz. Figure 6(a) illustrates that although the WVASE model overpredicts reflectance, the qualitative agreement between the WVASE-predicted reflectance and the measured value is quite good. This overprediction is especially strong in the region of the π plasmon. The π plasmon exhibits highly anisotropic behavior in single and aligned SWCNTs,[44,45] and some of the discrepancy between the measured and modeled reflectance may be attributable to the isotropic approximation used in the optical model.

Although the agreement between the measured and calculated transmittances shown in Fig. 6(b) is not ideal, the model does predict the important features in the measured

transmission spectrum. As with the reflectance spectra, the measured and modeled transmittances show good qualitative agreement. The model overpredicts reflectance by about 7%–8%, which is likely a large contributor to the discrepancy in absolute transmission intensity. Both the model-predicted and experimentally measured data show significant losses in the range between 3.5 and 5.5 eV, which are attributable to the π plasmon. However, the transmission minimum is shifted from 4.4 eV in the measured data to 4.7 eV in the model-predicted transmittance. This shift is difficult to detect in the reflectance data, but it is readily apparent in the absorption spectra. High transmission in the visible and near-ultraviolet energy range is critical to many optoelectronic applications, and these data strongly indicate that optical losses caused by the π plasmon are detrimental to visible light transmission.

Measured absorption and the WVASE-model-predicted absorption spectra are presented in Fig. 6(c). Absorption was experimentally determined by subtracting the measured transmittance and reflectance from unity (i.e., $A = 1 - T - R$). Figure 6(c) illustrates that the experimentally determined absorption and the measured data show good agreement. However, the position of the π plasmon is shifted by 0.3 eV in the model-predicted absorption spectrum with respect to the measured absorption data. This shift is consistent with the discrepancy between the locations of the π-plasmon peak in ε_2 (4.75 eV) and the minimum in the measured transmittance (4.44 eV). Comparing Fig. 6(a) with Fig. 6(c) demonstrates that absorbance is much larger than reflectance in the SWCNT networks. This indicates that neglecting reflectance when determining the absorbance introduces an error of 5%–10%, which may be an acceptable approximation for many applications.

The optical constants generated from the ellipsometry model suggest a strong reflectance peak at the π plasmon, which is not experimentally observed in the spectrophotometry data. To better understand the reflectance of SWCNTs and the effects of anisotropy, angularly dependent reflectance measurements were performed on the M-2000 ellipsometer with p- and s-polarized light. Briefly, the electric-field vector of p-polarized light lies in the plane of incidence, and the electric-field vector of s-polarized light is normal to the plane of incidence. At normal incidence, both polarizations are parallel to the substrate plane. As the angle of incidence increases, the component of the p polarization in the substrate plane decreases, while the s polarization continues to be parallel to the sample plane. The data presented in Fig. 7 show the measured (a) p- and (b) s-polarized reflection spectra and model-predicted (c) p- and (d) s-polarized reflectance spectra for angles between 15° and 75°.

The p-polarized reflection spectra given in Fig. 7(a) show the expected monotonic decrease in intensity between 15° and 55°, along with a strong increase in intensity at 65° and 75° caused by passing beyond Brewster's angle for the SWCNT network. The overall reflection intensity is stronger at high angles of incidence due to predictable effects, but contributions from the π plasmon become especially strong at high angles for p-polarized light. The strong reflection peak at high angles suggests that an electric field normal to the substrate plane couples more strongly than an electric
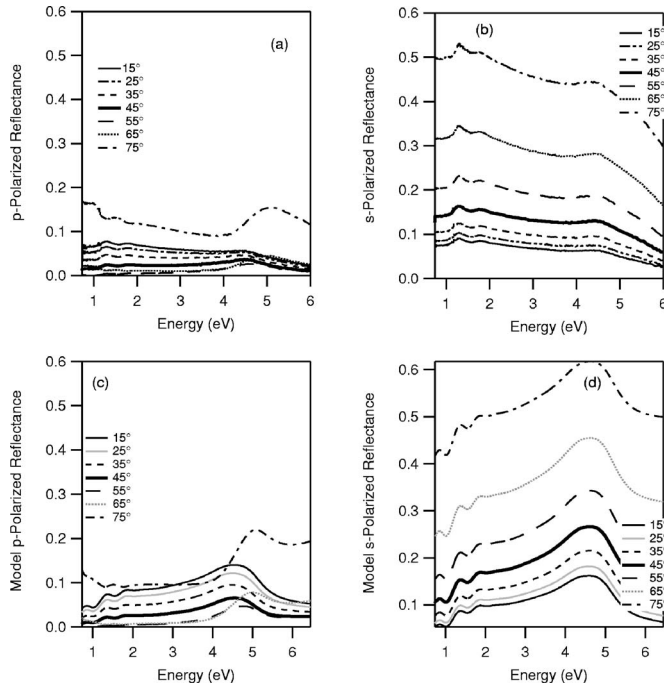
FIG. 7. Angle-dependent reflectance spectra for a 50 Ω/sq film on quartz. Measured reflection spectra were taken on the M-2000 ellipsometer using (a) *p*- and (b) *s*-polarized light at angles varying from 15° to 70°. The modeled data points for (c) *p*- and (d) *s*-polarized reflection spectra were calculated using WVASE from the Ψ, Δ, and *T* data and without fitting to the reflection data.

field in the substrate plane. This is somewhat counterintuitive for SWCNT networks. The π plasmon is expected to oscillate along the nanotube axis,[24] which, according to Fig. 1, lies primarily in the substrate plane. Figure 6(c) shows a strong absorption in the π plasmon region at normal incidence, which is in agreement with the literature data and indicative of strong coupling between the π plasmon and an electric-field vector parallel to the nanotube axis. The reflectance spectra indicate that some amount of coupling with a normal electric field is also occurring, and this behavior is not well understood.

Figure 7(b) shows the angularly dependent *s*-polarized reflection data. These data show a monotonic increase with increasing angle of incidence that is expected from most materials. However, there is only a small contribution from the π plasmon to the *s*-polarized reflectance. The minimal presence of the π-plasmon peak in these spectra is also somewhat unexpected. The *s*-polarized electric-field vector always remains in the substrate plane, yet it shows minimal coupling with the π plasmon in the reflectance spectrum. Overall reflection intensities are much higher than for the *p*-polarized light. Previous work suggests that the π plasmon exhibits a strong angular and polarization dependence,[44,45] which is consistent with the data shown in Figs. 7(a) and 7(b).

In contrast to the effect on the π plasmon, the peaks due to the E_s^{11}, E_s^{22}, and E_m^{11} transitions are relatively unaffected by the change in polarization. This is because they are localized excitonic transitions occurring in the individual tubes.[24] There are no interactions between the tubes or delocalization due to these transitions, which makes them less sensitive to

angle or polarization. The spectra from the *p*- and *s*-polarized reflectance measurements are similar at low angles of incidence (<45°) and then deviate strongly at high angles. At near-normal angles of incidence, both the *s*- and *p*-wave vectors are in the plane of the sample, likely contributing to the relatively small reflectance from the π plasmon at low angles for both polarizations.

The modeled data in Figs. 7(c) and 7(d) were generated using the optical constants and model, which were determined from fits to the Ψ and Δ data shown in Fig. 4. No additional fitting to the angularly dependent reflectance data was performed. Figure 7 shows significant discrepancies between the model-predicted and measured reflectances, but the model captures the essential features of the angular dependence without any additional fitting for the *p*-polarized reflection spectra. The measured reflectance is significantly higher at high angles, and the reflection in the region of the π plasmon becomes especially large at 65° and 75°. The measured reflectance is small at low angles, which indicates that, as is shown in Fig. 6(a), reflection at normal incidence should be small. The model does predict a higher reflectance from the π plasmon at low angles of incidence than is experimentally observed.

Comparison of Figs. 7(d) and 7(b) shows that the optical model predicts the reflection intensity and dependence on angle of incidence fairly well. However, the model predicts a large reflection of *s*-polarized light from the π plasmon. This reflection is not experimentally observed, and the mismatch between the model-predicted and measured data sets suggests that the model fails to capture the polarization dependence of the π-plasmon oscillation. This further supports the idea that the optical properties of SWCNT films are highly anisotropic, and that the isotropic approximation introduces some error into the optical model. Future development of the optical model will require the incorporation of anisotropy.

IV. CONCLUSIONS

Electrical characterization indicates that the conduction mechanism of the SWCNT networks under study is strongly affected by *p*-type semiconducting tubes that are interconnected with metallic tubes. This interpretation is supported by device data where SWCNT networks were successfully employed as hole-conducting electrodes in organic PV devices.[7] Poor electrical contact between tubes appears to limit the conductivity in the networks. The SWCNT thin films are essentially hole conducting and highly transparent, which is a desirable and previously unobtainable combination of properties for use in photovoltaics.

The combined VASE and spectrophotometry data show that fundamental transitions of SWCNT appear responsible for a significant fraction of the optical losses in these electrodes. However, various modifications or chemical treatments may be used to reduce some of the losses through doping.[12,46] The data also show that most of the losses are due to absorption and that absorption likely caused by the π plasmon contributes strongly to the poor transparency in the near-ultraviolet and visible portions of the spectrum. Work is ongoing to determine optimum doping and other techniques

to improve the SWCNT electrodes for use in PV devices.

The optical constants presented here predict well the optical transmission, reflection, and absorption of the networks, but there are discrepancies in the absolute value of the transmittance and reflectance. The overprediction of reflectance may be due to the anisotropic behavior of the material in the region of the π-plasmon oscillation. This will be addressed with the incorporation of optical anisotropy in future work. Despite this overprediction, the agreement between the optical model and measured optical properties is still fairly good. These results show that it is reasonable to use an isotropic approximation to model the optical properties of SWCNT electrodes, but that an anisotropic model would likely be much more accurate.

In conclusion, we show that the SWCNT electrodes have exceptionally promising optoelectronic properties for use in PV devices. The availability of a p-type transparent electrical contact could significantly advance the field of thin-film tandem solar cells and is of great use in organic solar cells. So far, devices made with SWCNT electrodes replacing conventional TCOs have had slightly lower efficiencies. However, manipulation of the optical properties through chemical doping appears promising. We show that variable-angle spectroscopic ellipsometry is a very useful tool for studying SWCNT film properties. We demonstrate an optical model that captures the essential features of the film reflection and transmission spectra and agrees well with previously published results from other methods.

[1] D. S. Ginley and C. Bright, MRS Bull. **25**, 15 (2000).

[2] T. J. Coutts, J. S. Ward, D. L. Young, K. A. Emery, T. A. Gessert, and R. Noufi, Prog. Photovoltaics **11**, 359 (2003).

[3] Zhuangchun Wu, Chen Zhihong, Du Xu, J. M. Logan, J. Sippel, M. Nikolou, K. Kamaras, J. R. Reynolds, D. B. Tanner, A. F. Hebard, and A. G. Rinzler, Science **305**, 1273 (2004).

[4] G. Fanchini, H. E. Unalan, and M. Chhowalla, Appl. Phys. Lett. **88**, 191919 (2006).

[5] X. Yu, R. Rajamani, K. A. Stelson, and T. Cui, J. Nanosci. Nanotechnol. **6**, 1939 (2006).

[6] G. Grüner, J. Mater. Chem. **16**, 3533 (2006).

[7] J. van de Lagemaat, T. M. Barnes, G. Rumbles, S. E. Shaheen, T. J. Coutts, C. Weeks, I. Levitsky, J. Peltola, and P. Glatkowski, Appl. Phys. Lett. **88**, 233503 (2006).

[8] M. W. Rowell, M. A. Topinka, M. D. McGehee, H. J. Prall, G. Dennler, N. S. Sariciftci, L. B. Hu, and G. Grüner, Appl. Phys. Lett. **88**, 233506 (2006).

[9] M. Contreras, T. M. Barnes, J. van de Lagemaat, G. Rumbles, T. J. Coutts, C. Weeks, P. Glatkowski, I. Levitsky, and J. Peltola, IEEE Fourth World Conference on Photovoltaic Energy Conversion, Waikoloa, HI, 2006. NREL Report No. CP-520-39914.

[10] K. Lee, Z. Wu, Z. Chen, F. Ren, S. J. Pearton, and A. G. Rinzler, Nano Lett. **4**, 911 (2004).

[11] R. Saito, G. Dresselhaus, and M. S. Dresselhaus, *Physical Properties of Carbon Nanotubes*, 1st ed. (Imperial College Press, London, 1998).

[12] V. Skakalova, A. B. Kaiser, U. Dettlaff-Weglikowska, K. Hrncarikova, and S. Roth, J. Phys. Chem. B **109**, 7174 (2005).

[13] P. G. Collins, K. Bradley, M. Ishigami, and A. Zettl, Science **287**, 1801 (2000).

[14] D. S. Hecht, L. Hu, and G. Grüner, Appl. Phys. Lett. **89**, 133112 (2006).

[15] A. B. Kaiser, Y. W. Park, G. T. Kim, E. S. Choi, G. Dusberg, and S. Roth, Synth. Met. **103**, 2547 (1999).

[16] V. Skakalova, A. B. Kaiser, Y.-S. Woo, and S. Roth, Phys. Rev. B **74**, 085403 (2006).

[17] L. Hu, D. S. Hecht, and G. Grüner, Nano Lett. **4**, 2513 (2004).

[18] U. Dettlaff-Weglikowska, V. Skakalova, R. Graupner, S. H. Jhang, B. H. Kim, H. J. Lee, L. Ley, Y. W. Park, S. Berber, D. Tomanek, and S. Roth, J. Am. Chem. Soc. **127**, 5125 (2005).

[19] A. B. Kaiser, G. Dusberg, and S. Roth, Phys. Rev. B **57**, 1418 (1998).

[20] X. Liu, T. Pichler, M. Knupfer, M. S. Golden, J. Fink, H. Kataura, and Y. Achiba, Phys. Rev. B **66**, 045411 (2002).

[21] H. Kataura, Y. Kumazawa, Y. Maniwa, I. Umezu, S. Suzuki, Y. Ohtsuka, and Y. Achiba, Synth. Met. **103**, 2555 (1999).

[22] B. J. Landi, H. J. Ruf, C. M. Evans, C. D. Cress, and R. P. Raffaelle, J. Phys. Chem. B **109**, 9952 (2005).

[23] X. Liu, T. Pichler, M. Knupfer, M. S. Golden, J. Fink, D. A. Walters, M. J. Casavant, J. Schmidt, and R. E. Smalley, Synth. Met. **121**, 1183 (2001).

[24] T. Pichler, M. Knupfer, M. S. Golden, J. Fink, A. Rinzler, and R. E. Smalley, Phys. Rev. Lett. **80**, 4729 (1998).

[25] M. Kaempgen, G. S. Duesberg, and S. Roth, Appl. Surf. Sci. **252**, 425 (2005).

[26] C. M. Trottier, P. Glatkowski, P. Wallis, and J. Luo, J. Soc. Inf. Disp. **13**, 759 (2005).

[27] I. W. Chiang, B. E. Brinson, R. E. Smalley, J. L. Margrave, and R. H. Hauge, J. Phys. Chem. B **105**, 1157 (2001).

[28] H. Hu, B. Zhao, M. E. Itkis, and R. C. Haddon, J. Phys. Chem. B **107**, 13838 (2003).

[29] D. L. Young, T. J. Coutts, and V. I. Kaydanov, Rev. Sci. Instrum. **71**, 462 (2000).

[30] R. G. Gordon, MRS Bull. **25**, 52 (2000).

[31] S. K. M. Jonsson, J. Birgerson, X. Crispin, G. Greczynski, W. Osikowicz, A. W. D. van der Gon, W. R. Salaneck, and M. Fahlman, Synth. Met. **139**, 1 (2003).

[32] M. Stadermann, S. J. Papadakis, M. R. Falvo, J. Novak, E. Snow, Q. Fu, J. Liu, Y. Fridman, J. J. Boland, R. Superfine, and S. Washburn, Phys. Rev. B **69**, 201402(R) (2004).

[33] J. E. Fischer, H. Dai, A. Thess, R. Lee, N. M. Hanjani, D. L. Dehaas, and R. E. Smalley, Phys. Rev. B **55**, R4921 (1997).

[34] J. Vavro, J. M. Kikkawa, and J. E. Fischer, Phys. Rev. B **71**, 155410 (2005).

[35] H. E. Romero, K. Bolton, A. Rosen, and P. C. Eklund, Science **307**, 89 (2005).

[36] K. Bradley, J.-C. P. Gabriel, and G. Grüner, Nano Lett. **3**, 1353 (2003).

[37] E. S. Snow, J. P. Novak, P. M. Campbell, and D. Park, Appl. Phys. Lett. **82**, 2145 (2003).

[38] C. M. Aguirre, S. Auvray, S. Pigeon, R. Izquierdo, P. Desjardins, and R. Martel, Appl. Phys. Lett. **88**, 183104 (2006).

[39] B. Johs, C. Herzinger, and B. Guenther, WVASE for Windows 3.511, J. A. Woolam Co., Lincoln, NE, 2005.

[40] Charles C. Kim, J. W. Garland, H. Abad, and P. M. Raccah, Phys. Rev. B **45**, 11749 (1992).

[41] F. Borondics, K. Kamaras, M. Nikolou, D. B. Tanner, Z. H. Chen, and A. G. Rinzler, Phys. Rev. B **74**, 045431 (2006).

[42] *Guide to Using WVASE32* (J. A. Woolam Co., Inc., Lincoln, NE, 2001).

[43] A. Gruneis, R. Saito, G. G. Samsonidze, T. Kimura, M. A. Pimenta, A. Jorio, A. G. Souza Filho, G. Dresselhaus, and M. S. Dresselhaus, Phys. Rev. B **67**, 165402 (2003).

[44] J. Hwang, H. H. Gommans, A. Ugawa, H. Tashiro, R. Haggenmueller, K. I. Winey, J. E. Fischer, D. B. Tanner, and A. G. Rinzler, Phys. Rev. B **62**, R13310 (2000).

[45] Y. Murakami, E. Einarsson, T. Edamura, and S. Maruyama, Phys. Rev. Lett. **94**, 087402 (2005).

[46] R. Jacquemin, S. Kazaoui, D. Yu, A. Hassanien, N. Minami, H. Kataura, and Y. Achiba, Synth. Met. **115**, 283 (2000).